The Journal of Chemical Physics

Single-spin vector analysis of strongly coupled nuclei in TOCSY NMR experiments

Cite as: J. Chem. Phys. **151**, 134117 (2019); https://doi.org/10.1063/1.5123046
Submitted: 02 August 2019 . Accepted: 12 September 2019 . Published Online: 07 October 2019

Anders B. Nielsen, Michael Ryan Hansen, Jørgen Ellegaard Andersen, and Thomas Vosegaard

AIP Publishing

The Journal of Chemical Physics ARTICLE scitation.org/journal/jcp

Single-spin vector analysis of strongly coupled nuclei in TOCSY NMR experiments

Cite as: J. Chem. Phys. 151, 134117 (2019); doi: 10.1063/1.5123046
Submitted: 2 August 2019 • Accepted: 12 September 2019 •
Published Online: 7 October 2019

Anders B. Nielsen,[1,2,a)] Michael Ryan Hansen,[3] Jørgen Ellegaard Andersen,[1,4] and Thomas Vosegaard[1,2,a)]

AFFILIATIONS

[1]Interdisciplinary Nanoscience Center (iNANO), Aarhus University, Gustav Wieds Vej 14, DK-8000 Aarhus C, Denmark
[2]Department of Chemistry, Aarhus University, Gustav Wieds Vej 14, DK-8000 Aarhus C, Denmark
[3]Institute for Physical Chemistry, Westfälische Wilhelms-Universität Münster, Corrensstrasse 28/30, D-48149 Münster, Germany
[4]Department of Mathematics, Center for Quantum Geometry of Moduli Spaces, Ny Munkegade 118, DK-8000 Aarhus C, Denmark

[a)]**Authors to whom correspondence should be addressed:** abn@inano.au.dk and tv@chem.au.dk

ABSTRACT

This paper presents a new way to represent the effect of complex radio-frequency (rf) pulse sequences on J-coupled nuclear spin systems. The model uses a vector representation of the single-spin interactions (chemical-shift and rf interactions) and provides a simple route to gain analytical insight into multipulse NMR experiments. The single-spin Hamiltonian is expressed in an interaction representation as Fourier components. These Fourier components are combined for the two spins to establish the averaged coupling term of the Hamiltonian. This effective Hamiltonian is fast to calculate as only single-spin rotations are used and followed by simple summation of numbers for reconstruction of given coupling interactions. The present method is used to gain analytical insight into the performance of the J-coupling transfer sequence DIPSI-2 through two figures of merit (FOM) providing useful information for optimization of such pulse sequences. The first FOM (Ξ_{AB}) reports the efficiency of the desired total correlation spectroscopy transfer and should be as large as possible, while the second (Ξ_{Het}) reports the potential leakage of coherence to a heteronuclear spin and should be as small as possible.

INTRODUCTION

Since the early days of NMR, researchers have benefitted from the tight coupling between the theoretical description of NMR and the experimental observations.[1] This has enabled a precise theoretical description of most experimental observables, e.g., relaxation by the Redfield formalism[2] and manipulations of coupled spins by radio-frequency (rf) pulse sequences using the product-operator formalism by Sørensen *et al.*[3] However, it is not always possible to work out an analytical description for a given problem, which is why substantial efforts have also been devoted to the development of software implementing numerical simulations of NMR experiments.[4–11] This approach can in many cases provide good insight into the function of pulse sequences and their dependency on various parameters, stability toward experimental artefacts, etc. However, in some cases, even though such valuable information is available from numerical simulations, it is difficult to use the results of numerical simulations to provide generalized conclusions on the performance of the experiments in question. To do this, it is necessary to bridge the gap between simple analytical solutions and numerical simulations of complex experiments and establish analytical insight into such experiments.

Homonuclear coherence transfer in total correlation spectroscopy (TOCSY) experiments[12,13] are good examples of a class of experiments where the performance highly depends on the choice of pulse sequence and the observed spin system. It is further desirable to establish broadband pulse sequences that maintain a high scaling factor for the J coupling. To achieve this, advanced pulse sequences have been developed,[13–16] and over the years, new TOCSY mixing sequences have been presented to obtain better transfer efficiencies,[17–19] selectivity[20,21] reduced power mixing,[22] or other specific purposes.[23–27] These developments have been supported by numerical simulations[28] or Floquet theory,[29] providing insight into the function of the transfer block. A common trait is, however, that

efficient homonuclear cross-polarization sequences used to mediate the homonuclear coherence transfer in TOCSY need numerical simulations to get full insight.

Recently, we presented and proposed a strategy for handling the effect of chemical shift in the theoretical description of dipolar recoupling experiments.[30] This strategy involved handling the combined effect of rf and chemical shift for each nucleus by moving into an interaction frame that included these effects and then describing the dipolar coupling in these interaction frames. While this approach greatly simplified the description of complex pulse sequences and provides new analytical insight, it involved a number of resonance and near-resonance conditions that could complicate the description.

Here, we simplify and improve this approach. The simplification is that we will use a simple Bloch vector representation for the single-spin interactions. The improvement is that we introduce a second interaction frame that completely removes the notation of resonance and near-resonance conditions. From the simple vector representation of single spins, we are able to calculate the effect of any periodic pulse sequence on the individual spins, establish an expression for the average Hamiltonian, and then combine the obtained information to establish expressions for two-spin interactions. The interactions related to a single spin [chemical shift and radio-frequency (rf) interactions] provide a net rotation of the density operator around through what we call the effective field of the pulse sequence. By establishing an interaction-frame description that compensates this effective field, we may express the effect of the total Hamiltonian (including the two-spin J-coupling) as a simple expansion of Fourier components in the basis of the modulation frequency of the pulse sequence. As a second step to simplify the description, we calculate the average Hamiltonian from the Fourier components, leading to a very simple description of the total Hamiltonian.

While the single-spin vector description is general and may be used to describe any pulse sequence, we have here chosen to analyze different TOCSY mixing sequences. We find that for any of these mixing sequences, the homonuclear two-spin average Hamiltonian resembles the Hamiltonian of the well-known strongly coupled AB spin system.[31] With this insight, we may readily obtain expressions for the scaling factor of the J coupling and thereby a simple measure for the figure of merit (FOM) for the given pulse sequence. Finally, we use the present method to predict the influence of heteronuclear couplings on the TOCSY mixing.

THEORY

The essence of this section is to determine the effect of the chemical shift and rf interactions on each spin in a two-spin system, move into an interaction frame[32] handling this effective field, expressing the two-spin J coupling term in these interaction frames, and finally calculating the average J coupling Hamiltonian over the period of the pulse sequence.

The Hamiltonian relevant for a homonuclear J-based transfer includes chemical shift, J-coupling, and (rf) pulses. This Hamiltonian may be expressed as follows:

$$\widehat{H}(t) = \Omega_1\hat{I}_{1z} + \Omega_2\hat{I}_{2z} + \pi J 2\hat{I}_1 \cdot \hat{I}_2 + \omega_{\mathrm{rf}}(t)\left[\left(\hat{I}_{1x} + \hat{I}_{2x}\right)\cos\theta(t) + \left(\hat{I}_{1y} + \hat{I}_{2y}\right)\sin\theta(t)\right] \quad (1)$$

in the rotating frame and with the standard shorthand nomenclature $\hat{I}_1 \cdot \hat{I}_2 = \hat{I}_{1,x} \otimes \hat{I}_{2,x} + \hat{I}_{1,y} \otimes \hat{I}_{2,y} + \hat{I}_{1,z} \otimes \hat{I}_{2,z}$. The Hamiltonian in Eq. (1) enters the Liouville-von-Neumann equation establishing the time evolution of the density operator $\hat{\rho}'(t) = -i[\hat{H}(t), \hat{\rho}(t)]$ or the propagator $\hat{U}'(t) = -i\hat{H}(t)\hat{U}(t)$. These equations give the solution $\hat{\rho}(t) = \hat{U}(t)\hat{\rho}(0)\hat{U}^{-1}(t)$, where $\hat{U}(t) = \hat{T}e^{-i\int_0^t \hat{H}(t')dt'}$ and $\hat{T}$ is the Dyson time-ordering operator.

The rotating frame refers to a frame that rotates around z in the laboratory frame with the carrier frequency, corresponding to the base frequency of the rf pulses. The first two terms represent the chemical shifts, or more precisely, Ω_j represents the frequency difference between the chemical shift of nucleus j and the rotating frame. If off-resonance pulses are applied (i.e., pulses with a different base frequency than the carrier frequency), these may be described by changing the pulse phase according to $\theta(t) = \theta_{\mathrm{rf}}(t) + \omega_{\mathrm{off}}t$. Henceforth, we will represent the rotating frame by the letter R.

The single-spin vector procedure involves five steps:

I. Express the single-spin operators in the interaction frame of the single-spin Hamiltonian terms (rf and chemical shift interactions).
II. Determine the overall effect (rotation axis and rotation angle) of the single-spin Hamiltonian, the *effective rotation*.
III. Define a new set of single-spin operators that are aligned with the effective coordinate system of the pulse sequence (z_{eff} is the effective rotation axis of the pulse sequence) and a set of single-spin operators that rotate around the effective coordinate axis with the effective frequency.
IV. Decompose the description of the interaction-frame operators to a sum of periodic time-dependent terms and time-independent terms.
V. Establish the effective J coupling from the effective single-spin operators.

When applying this decomposition procedure to describe the J-coupling interaction, we can obtain immediate insight into the mode of action of even complex pulse sequences, which in this work is exemplified by investigation of isotropic mixing sequences for J-coupling mediated transfer in TOCSY experiments. While the five steps allow us to establish a very simple insightful description of complex pulse sequences, obtaining the actual expressions of the periodic decomposition is somewhat difficult and involves defining several interaction frames and projection frames. The necessary derivations are given in the Appendix and will be briefly explained below. To support the derivations, the supplementary material provides a mathematical proof of the correctness of the derivations.

To investigate the effect of a pulse sequence for a given spin system, we will first consider a single spin and then establish the J-coupling Hamiltonian afterward. The single-spin Hamiltonian contains the terms of the chemical shift and rf pulses, but no J coupling and is given by [disregarding the nucleus index in Eq. (1) for simplicity, i.e., $\hat{I}_x \equiv \hat{I}_{1x}$, etc.]

$$\widehat{H}_{ss}(t) = \Omega\hat{I}_z + \omega_{\mathrm{rf}}(t)\left[\hat{I}_x\cos\theta(t) + \hat{I}_y\sin\theta(t)\right]. \quad (2)$$

The pulse sequence leads to a net (effective) rotation of the single-spin magnetization. We denote the axis as z^F referring to the z axis of the flipped frame as introduced in the Appendix. The effective rotation is given by $\chi_{\mathrm{eff}} = \omega_{\mathrm{eff}}t_M$, where we have introduced the

effective frequency of the pulse sequence ω_{eff} and the length of the pulse sequence, t_M.

When handling complex pulse sequences, it is convenient to express the Hamiltonian in the interaction frame of the pulse sequence. In our case, the interaction frame includes all terms of the single-spin Hamiltonian in Eq. (2) and is referred to as the single-spin interaction frame (S).

The next step is to express the single-spin interaction-frame operators in the flipped frame. This will allow us to remove the effective field in the same way that we move the description from the lab frame into the rotating frame, since the effective field creates a rotation around the z axis in the flipped frame. Performing this transformation, the effective rotation is removed from the time dependence of the pulse sequence and introduced as a Coriolis term. The frame that rotates around z^F with the effective frequency is labeled the Effective frame (E). Combining single-spin vectors of the two spins for the full Hamiltonian [cf. Eq. (1)], we obtain

$$\tilde{\tilde{H}} = -\omega_{1,\text{eff}}\hat{I}^F_{1,z} - \omega_{2,\text{eff}}\hat{I}^F_{2,z} + \pi J \times \sum_{q,q',q''=x,y,z}\left(\sum_{k=-\infty}^{\infty} a^k_{1,q',q}a^{-k}_{2,q'',q}\right)2\hat{I}^F_{1,q'} \otimes \hat{I}^F_{2,q''}, \quad (3)$$

where the coefficients $a^k_{i,q,q'}$ are Fourier components of the time-dependent projections of the pulse sequence for the ith spin of the three axes $q = x, y, z$ as derived in the Appendix.

For a given pulse sequence, we may readily calculate the effective frequencies for all single-spin Hamiltonians and the Fourier components for J-coupled spin pairs to evaluate any surviving terms. In combination with the truncation due to the effective rotations, the Fourier components will allow us to easily calculate the scaling factor for the J coupling for any spin pair.

RESULTS AND DISCUSSION

The single-spin vector analysis presented in this paper can be used to understand the effect of pulse sequences acting on J-coupled spin systems. In the following, we will apply this theory to investigate the efficiency of a homonuclear decoupling scheme for coherence transfer during the mixing time of a TOCSY experiment. One of the most popular TOCSY mixing sequences is the DIPSI-2 pulse sequence.[15] It consists of nine pulses with pulse flip angles of 320°, 410°, 290°, 285°, 30°, 245°, 375°, 265°, and 370° with phases alternating between 0° and 180°. This block is supercycled four times using phases of 0°, 0°, 180°, and 180° and has a total length of t_M and $N = 9 \times 4 = 36$ pulse elements. This pulse sequence is illustrated in Fig. 1(a), where the nine pulses are represented by lines and with phases shown for in the expansion of the first supercycle. During each pulse, the Hamiltonian is time-independent and may be described by a single rotation quaternion.

The essence of the present single-spin vector analysis is to move the description of the pulse sequence into an interaction frame, where the time-modulation of the pulse sequence is made cyclic over the period (t_M) of the pulse sequence. To highlight the individual steps, Fig. 1(b) shows the time evolution of the single-spin interaction frame [i.e., the interaction frame that includes the rf

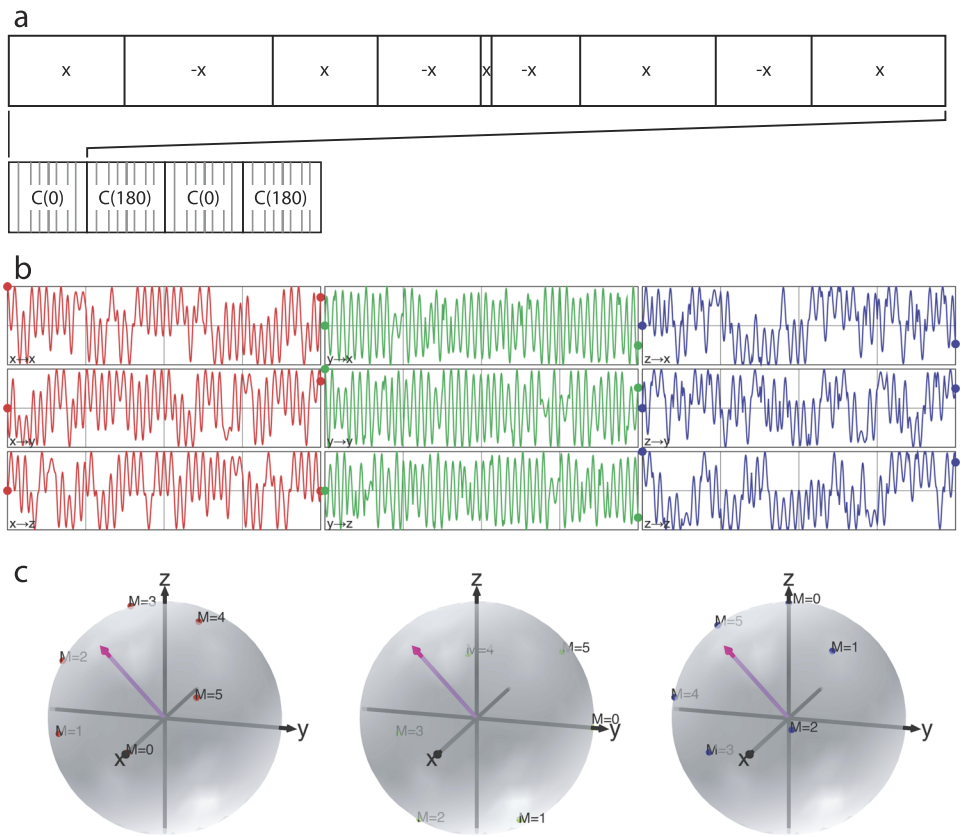

FIG. 1. (a) Timing scheme of the homonuclear DIPSI-2 pulse sequence. (b) Plots of the time evolution of the matrix $R^{SR}(t)$ during the DIPSI-2 pulse sequence. (c) Rotating-frame representation of the effective rotation performed by the DIPSI-2 sequence for a setup with start operators $\hat{\rho}(0) = \hat{I}_x$ (left), $\hat{I}_y$ (middle), and $\hat{I}_z$ (right) and for $M = 0$–5 DIPSI-2 blocks. All simulations employed an rf-field strength of 5 kHz and a chemical shift of $\Omega = 5.6$ kHz.

pulses and isotropic chemical shift, the single-spin Hamiltonian of Eq. (2)] in the rotating frame (cf. the Appendix and Fig. 5 for definitions of the frames). In Fig. 1(b), the labels $q \rightarrow p$ ($p, q = x, y, z$) mean the projection of axis q^S of the single-spin interaction frame onto axis p^R of the rotating frame. Following the introduction of rotation matrices given in the Appendix, the plots in Fig. 1(b) show the time evolution of the entries of the matrix $R^{SR}(t)$ introduced in Eq. (A5). In Fig. 1(b) the spin has a chemical shift of $\Omega/2\pi = -5.6$ kHz and experiences an rf-field strength of $\omega_{rf}/2\pi = 5.0$ kHz. It is not straightforward to identify the effective rotation axis from this plot, but the quaternion description derived in the Appendix provides a perfect tool for this. Figure 1(c) shows the time-evolution starting with operator states $\hat{\rho}(0) = \widetilde{\hat{I}}_x^S$, $\widetilde{\hat{I}}_y^S$, and $\widetilde{\hat{I}}_z^S$ as a function of the number of DIPSI-2 blocks (M). These plots also show the effective axis of the DIPSI-2 pulse sequence for this particular chemical shift as a magenta arrow. It is evident from these plots that the single-spin interaction-frame operators are indeed rotated around the effective axis by the pulse sequence.

The next step in the analysis is to define the flipped frame, which has its z axis along the effective axis of the pulse sequence, and to "unwind" the effective rotation. Figure 2 shows the trajectories of the single-spin operators in the different frames as explained below

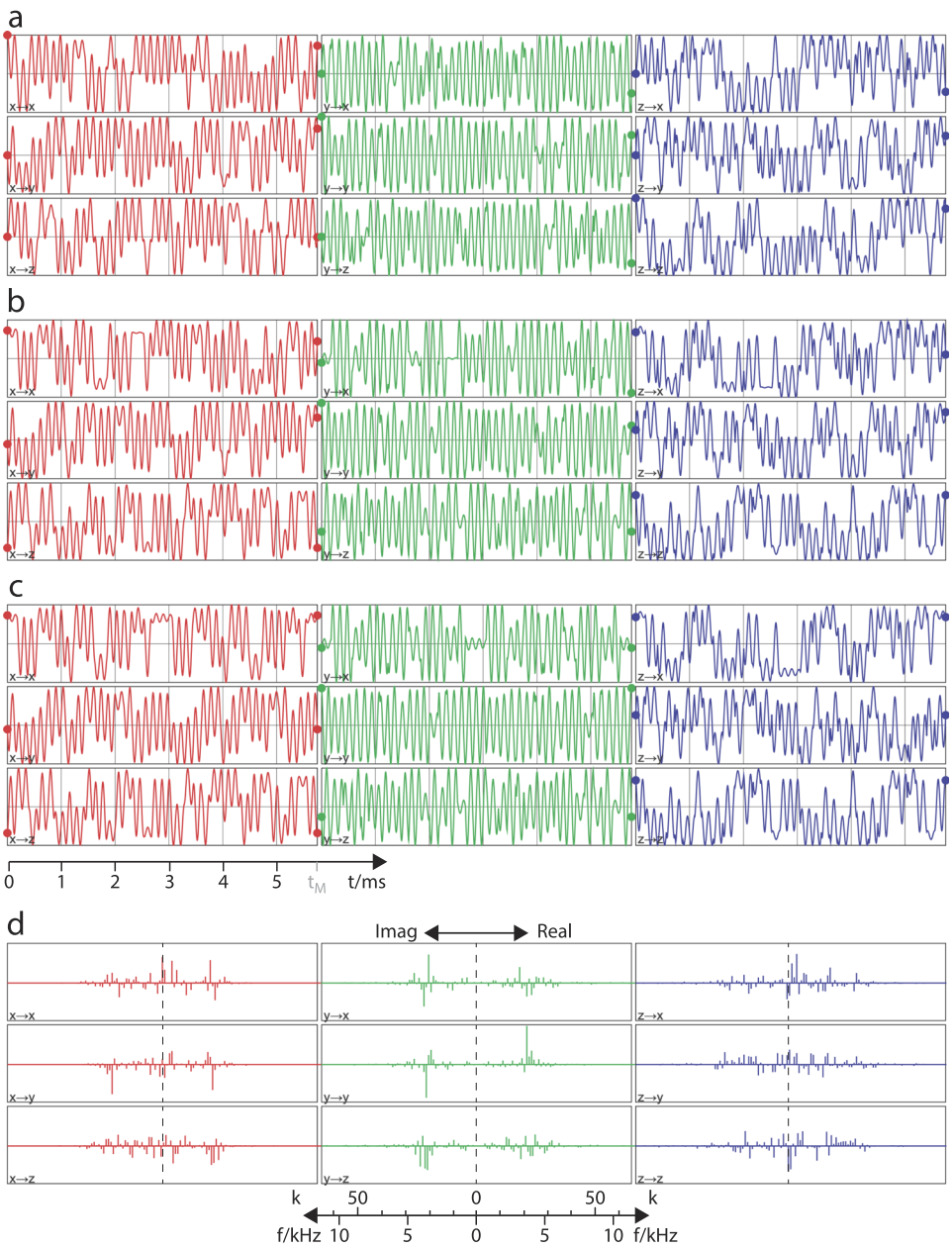

FIG. 2. Time evolutions of different projections of the single-spin interaction-frame operators. The relevant projections are onto (a) the rotating frame, (b) the flipped frame, and (c) the effective frame. Note that in the effective frame, all projections are cyclic with period t_M. (d) Fourier components of the projections of the single-spin interaction-frame operators in the effective frame expanded with the basic frequency $\omega_M/2\pi$. Here, f denotes the frequency of the Fourier components and k is the index. All simulations employed an rf-field strength of $\omega_{rf}/2\pi = 5$ kHz and a chemical shift of $\Omega = 5.6$ kHz.

and provides a nice overview of the process: Fig. 2(a) shows the projections onto the rotating frame [identical to Fig. 1(b)] in which none of the trajectories are periodic (the start points and end points are different for all trajectories). In the flipped frame [Fig. 2(b)], the z components show cyclic trajectories, as the net rotation is around z^F. Figure 2(b) demonstrates this cyclicity, since the z components (bottom row) all have the same starting point and end-point. The representation in Fig. 2(b) is equivalent to plotting the time dependence of the elements of R^{SF} introduced in the Appendix. The final transformation into the effective frame [Fig. 2(c)] simply "unwinds" the effective rotation by subtracting this effective rotation from the overall rotation, corresponding to the projection matrix R^{SE} derived in the Appendix. This implies that in this frame, all nine projections are cyclic.

Given that each component in the projection of the single-spin operators onto the effective frame is cyclic, these components be expanded as a Fourier series of the basic frequency ω_M. The corresponding Fourier components are shown in Fig. 2(d) and are equivalent to the components $a^k_{i,q,q'}$ introduced in Eq. (3).

In order to calculate the Fourier components, we need to find an appropriate number of equidistant time points to describe the pulse sequence. We have developed an automatic algorithm to do this. First, the algorithm aims at finding the greatest common divisor of the lengths of the pulse elements. In the case of DIPSI-2, all pulse lengths may be described as products of 5° flips. If we divide the sequence into 5° steps, we find that the pulse sequence may be divided into 2072 equidistant pieces. Next, the algorithm performs the full single-spin vector analysis and checks for high-frequency Fourier components. The algorithm doubles the number of points until the appearance of high-frequency Fourier components is smaller than a threshold value (typically set to 0.5% of the highest component). In the case of DIPSI-2, it turns out that 2072 points are sufficient. The algorithm typically requires only a few milliseconds of computation time to find the appropriate number of points.

When inspecting the Fourier components for DIPSI-2 in Fig. 2(d), it is quite obvious that significantly fewer than the 2072 Fourier components are important, since most components have amplitudes close to zero. Reducing the number of components may give a significant speed-up of the calculations. We do not filter out any of the Fourier components at the single-spin operator level, but rather assess the products of components in Eq. (3) and only proceed with Fourier coefficients fulfilling

$$\left|a^k_{1,q',q}a^{-k}_{2,q'',q}\right| > th, \tag{4}$$

where the threshold is typically fixed at $th = 0.005$, since we find that such a threshold is a good compromise providing precise and fast calculation results. For DIPSI-2 under the present conditions and with different chemical shifts in the range -10 kHz $\leq \Omega_1/2\pi, \Omega_2/2\pi \leq 10$ kHz, the algorithm found that on average only 82 coefficients contribute. Hence, the sum over k in Eq. (3) only requires 82 evaluations, which amounts to only 4% of the 2072 pulse events.

Up to this point, we have described the proposed single-spin vector analysis to easily calculate the effective Hamiltonian. In the following, we will use this effective Hamiltonian to explain some of the characteristics of the DIPSI-2 experiments. To do so, we will in the following propose two different figures of merit (FOM) for TOCSY experiments that are easily obtainable from the present analysis.

It may be noted that the Fourier components enter in the J-coupling term of the effective average Hamiltonian in Eq. (A18) and introduce a scaling of the effective J coupling. This scaling depends on the size of the sum of Fourier coefficients,

$$A_{q',q''} = \sum_{q=x,y,z}\sum_k a^k_{1,q',q}a^{-k}_{2,q'',q}. \tag{5}$$

The expression for the effective average Hamiltonian in Eq. (3) has essentially the same form as the well-known Hamiltonian of a strongly coupled spin system, a so-called AB-spin system,[1] under free precession. The only differences are that the chemical shift terms are replaced by the effective frequencies and that the normal J-coupling is replaced by the effective J-coupling term in Eq. (3) scaled by the Fourier coefficients $A_{q',q''}$ and that the present Hamiltonian contains terms involving spin operators of the form $\hat{I}_{1,q}\hat{I}_{2,q'}$, where $q \neq q'$. Indeed, this expansion makes a precise description of the two-spin system. For dipolar couplings under magic-angle spinning, we have demonstrated that a similar representation leads to accurate simulation results.[30] However, the aim here is to simplify matters even more, so we hypothesize that the AB-spin system Hamiltonian using the effective J coupling is a good approximation for the present system. We will not use this approximation for precise numerical calculations, but we will use it to establish more qualitative measures of the performance of different pulse sequences.

In a strongly coupled AB spin system, the transfer $I_{1,z} \leftrightarrow I_{2,z}$ is given by $(J/Q)^2\sin^2\pi Qt$, with $Q^2 = J^2+\Delta\nu^2$, where $\Delta\nu$ is the chemical shift difference. Our aim is to transfer this knowledge to our system. Since the present shifts represent rotations around the effective axes for the two spins (along z in the flipped frame), and since these axes are in general not collinear for the two spins, we choose to represent the effective offset between two nuclei as the length of the vector difference between the effective rotations [cf. Eq. (A1)],

$$\Delta\nu_{\text{eff}} = \frac{1}{2\pi}\left|\omega_{1,\text{eff}}\vec{u}_{1,\text{eff}} - \omega_{2,\text{eff}}\vec{u}_{2,\text{eff}}\right|. \tag{6}$$

Furthermore, the elements $A_{q',q''}$ may be considered as the entries of a Cartesian matrix. Since all components appear in the average effective Hamiltonian for the J coupling, we assume that the Euclidian norm of the $A_{q',q''}$ matrix,

$$J_{\text{eff}} = \frac{J}{\sqrt{3}}\sqrt{\sum_{q',q''}\left(A_{q',q''}\right)^2}, \tag{7}$$

can be used to represent the effective J coupling for the homonuclear transfer in TOCSY. Inspired by the resemblance with an AB-spin system transfer, we propose the following FOM for our system:

$$\Xi_{\text{AB}} = \frac{J_{\text{eff}}}{\sqrt{J^2_{\text{eff}} + \Delta\nu^2_{\text{eff}}}} \tag{8}$$

to illustrate the transfer efficiency of the pulse sequence.

Figure 3 shows the different parameters as a function of the chemical shift for the DIPSI-2 pulse sequence using 5.0 kHz rf field strength. Figure 3(a) reports the effective offset $\Delta\nu_{\text{eff}}$ as a function of chemical shift offset from the carrier frequency (defined at zero). It

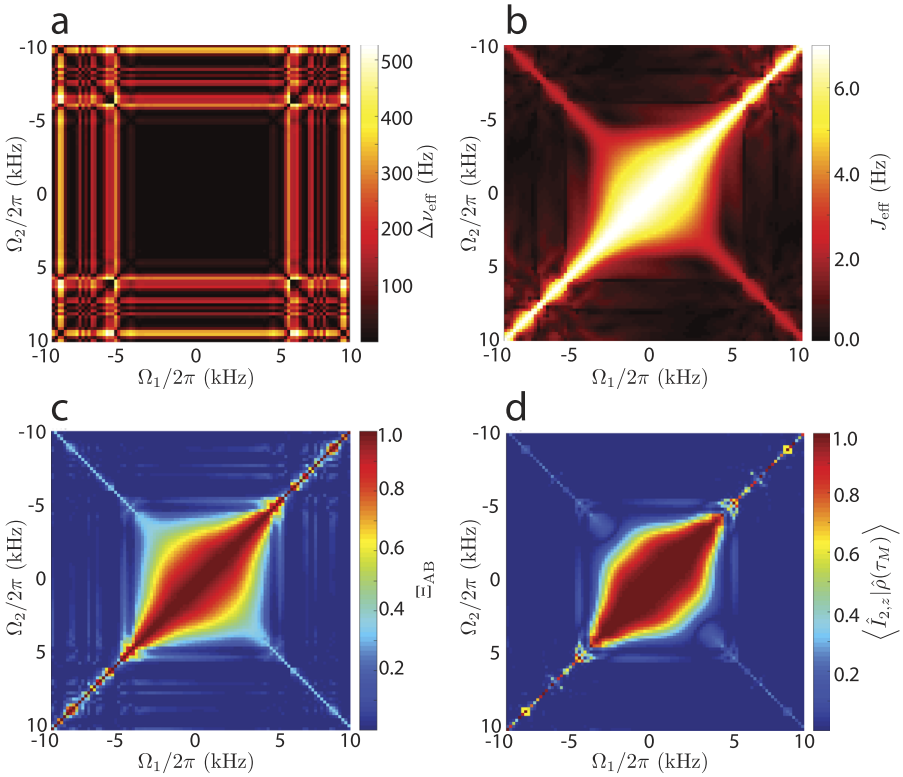

FIG. 3. Plots showing the performance of DIPSI-2. (a) The size of the effective offset between two nuclei, $\Delta\nu_{\mathrm{eff}}$. (b) The effective J coupling, J_{eff}. (c) The figure of merit Ξ_{AB}. (d) Numerical SIMPSON simulations showing the transfer efficiency $\hat{I}_{1,z} \rightarrow \hat{I}_{2,z}$ by using the DIPSI-2 pulse sequence for a mixing time of τ_M = 63.3 ms (corresponding to 11 DIPSI-2 blocks) and a J coupling of 7 Hz. All simulations employed an rf-field strength of 5 kHz.

can be seen that for the DIPSI-2 pulse sequence that the effective offset is almost zero within the chemical shift range similar to the used rf field strength for the DIPSI-2 pulse sequence. Figure 3(b) shows J_{eff} for chemical shift offsets in the same range reflecting the scaling factor of the J coupling encountered with DIPSI-2. Indeed, the effective J coupling scales down as the chemical shift difference between the two nuclei grows. TOCSY experiments require the J-coupling to be as strong as possible within the range of proton chemical shifts to be efficient. The FOM Ξ_{AB} is shown in Fig. 3(c). We anticipate that this FOM reflects the transfer efficiency of the pulse sequence. We note that for DIPSI-2 the shapes of the plots of J_{eff} and Ξ_{AB} are very similar, since $\Delta\nu_{\mathrm{eff}}$ is essentially zero in the range where J_{eff} is nonzero.

In order to verify the validity of the figure of merit Ξ_{AB}, we have numerically calculated the transfer efficiency in a homonuclear two-spin system using a starting operator $\hat{\rho}(0) = \hat{I}_{1z}$, a detecting operator $\hat{\rho}(\tau_M) = \hat{I}_{2z}$, and J = 7 Hz corresponding to a normal three-bond ^{1}H–^{1}H coupling using SIMPSON.[6,33] The numerical offset plot was done using a mixing time of 63.3 ms (corresponding to 11 DIPSI-2 elements). By comparing Figs. 3(c) and 3(d), it is seen that Ξ_{AB} captures all essential features of the numerically calculated offset plot. Hence, by performing two single-spin vector analysis calculations for the respective chemical shift offsets from the carrier frequency, we can reconstruct the effective (AB-spin system-like) Hamiltonian and hereby provide a simple measure for the transfer efficiency for a given pulse sequence by utilizing Eq. (8).

Finally, we introduce a second FOM which should not be regarded as a quality factor of the experiment but rather a measure of the amount of unwanted residual heteronuclear J-couplings under a homonuclear TOCSY transfer element. This situation may be relevant for uniformly ^{1}H, ^{13}C-labeled systems, where the undesired heteronuclear coupling can provide a means of leakage of magnetization from the protons. The heteronuclear J-coupling takes up the form $\hat{H}_J = \pi J 2\hat{I}_z \cdot \hat{S}_z$ in the high-field approximation. By applying a TOCSY element on the I channel, we will only observe a time-modulation of this spin-operator, while only the term $a^0_{S,z',z}$ is relevant for the S channel. With this knowledge and by using the single-spin vector method for the I channel, it is easy to write up the time-dependency of the heteronuclear coupling similar to Eq. (3). Since the terms combine according to Eq. (5), only the term $A^0_{z',z}$ is relevant for the heteronuclear coupling during a TOCSY sequence. Hence, we propose the following FOM as a measure of the scaling of a heteronuclear J-coupling Hamiltonian:

$$\Xi_{\mathrm{Het}} = abs(a^0_{I,z',z}). \tag{9}$$

Figure 4 illustrates the second FOM. In Fig. 4(a), the values for Ξ_{Het} calculated as a function of the isotropic chemical shift offset are reported. The chemical shift offset is on the channel where the DIPSI-2 pulse sequence is employed, and the DIPSI-2 sequence employs a 5.0 kHz rf field strength. It can be seen that within a range of approximately ±5 kHz offset, Ξ_{Het} is close to zero. This implies that the heteronuclear J-coupling under these circumstances will be averaged to zero (decoupled). As a guidance, one may assume that bad heteronuclear decoupling of the heteronuclear J-coupling is true whenever $\Xi_{\mathrm{Het}} > 0.5 J_{\mathrm{Homo}}/J_{\mathrm{Het}}$. Assuming typical values of J_{Het} = 130 Hz and J_{Homo} = 7 Hz (e.g., for $J_{\mathrm{Het}} = {}^1J_{\mathrm{CH}}$ and

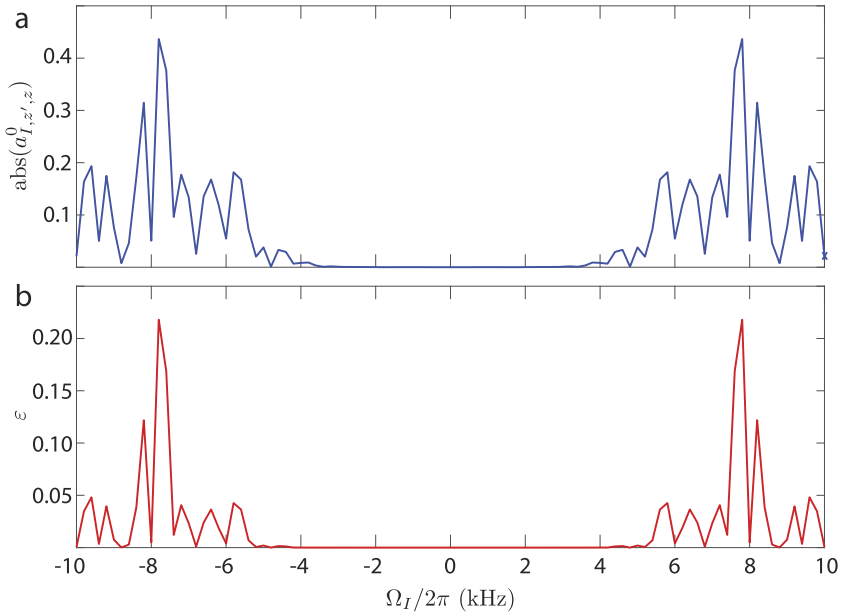

FIG. 4. (a) Plot of the magnitude for $\Xi_{\mathrm{Het}} = \mathrm{abs}(a^0_{1,z',z})$ as a function of the isotropic chemical shift offset for the DIPSI-2 pulse sequence with an rf-field strength of 5.0 kHz. (b) SIMPSON simulation showing the amount of signal lost for a heteronuclear two-spin system during DIPSI-2 employing an rf-field strength of 5.0 kHz on one channel and no pulses on the second channel (see text for further details).

$J_{\mathrm{Homo}} = {}^3J_{\mathrm{HH}}$), we find that poor heteronuclear decoupling is expected whenever $\Xi_{\mathrm{Het}} \gtrsim 0.025$. To validate if this is true, we have set up a numerical SIMPSON simulation for a heteronuclear two-spin system using a starting operator $\hat{\rho}(0) = \sum_{q=x,y,z} \hat{I}_{1q}$ and detecting the amount of signal lost after 11 entire DIPSI-2 blocks, corresponding to $\tau_M = 63.3$ ms. The signal loss was detected by the parameter $\varepsilon = 1 - \left\langle \sum_{q=x,y,z} \hat{I}_q | \hat{\rho}(\tau_M) \right\rangle$. The data from the simulations are presented in Fig. 4(b). By comparing the single-spin vector analysis with the numerical simulation [cf. Figs. 4(a) and 4(b)], we observe a precise correlation between these two datasets, appreciating that the resonance conditions are matched perfectly, and the intensity trends, which cannot be directly compared, also match quite well. This illustrates the strength of the single-spin vector analysis to provide insight into the spin dynamics of advanced pulse sequences. It should be noted that the present results show that in the particular case of DIPSI-2, heteronuclear couplings will have no practical relevance as the heteronuclear J-coupling is only active in offset ranges where the scaling factor of the homonuclear J coupling is essentially zero, so no homonuclear transfer would occur anyway.

CONCLUSION

In conclusion, we have presented a vector model to gain analytical insight into multipulse NMR experiments. The proposed model relies on a single-spin vector analysis performed on each nucleus in the spin system. The Fourier components for the average Hamiltonian found through this analysis are used to predict the performance of the pulse sequence for coupled spin-systems. The model provides a very fast way to calculate the effective Hamiltonian as only single-spin rotations are used and followed by simple summation of numbers for reconstruction of given coupling interactions. To exemplify the description, we have used the single-spin vector method to gain analytical insight into the performance of the J-coupling transfer sequence DIPSI-2. We have presented two figures of merit providing useful information for optimization of such pulse sequences. The first FOM (Ξ_{AB}) reports the efficiency of the desired TOCSY transfer and should be as large as possible, while Ξ_{Het} reports the potential leakage of coherence to a heteronuclear spin and should be as small as possible. These figures of merit only require single-spin calculations over the offset range of interest in order to validate the performance.

SUPPLEMENTARY MATERIAL

See supplementary material for the mathematical proof of the proposed double interaction-frame treatment of the Hamiltonians derived in the Theory section.

ACKNOWLEDGMENTS

We would like to thank the Danish Council for Independent Research (Grant No. DFF-4090-00223) and the Danish Ministry of Higher Education and Science (Grant No. AU-2010-612-181) for financial support. This work was partially supported by the center of excellence grant "Centre for Quantum Geometry of Moduli Spaces" from the Danish National Research Foundation (DNRF95).

APPENDIX: DERIVATION OF THE SINGLE-SPIN VECTOR ANALYSIS THEORY

The five steps involved in the single-spin vector analysis are associated mainly with a set of coordinate transformations that we will outline below. The relevant coordinate systems are shown in Fig. 5.

1. Interaction-frame representation of the single-spin operators

The single-spin Hamiltonian given in Eq. (2) is given by

$$\widehat{H}_{ss}(t) = \Omega \hat{I}_z + \omega_{\mathrm{rf}}(t)\left[\hat{I}_x \cos\theta(t) + \hat{I}_y \sin\theta(t)\right]. \quad \text{(A1)}$$

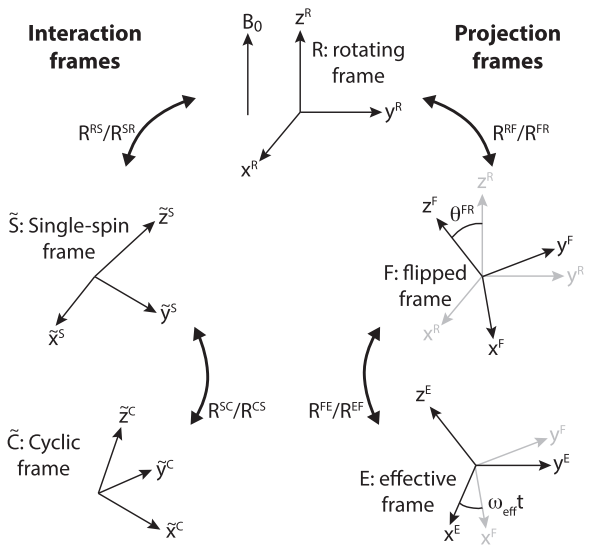

FIG. 5. Illustration of the different coordinate systems involved in the single-spin vector method. The rotating frame rotates around the z axis of the laboratory frame (not shown) with the carrier frequency. The flipped frame has its z axis aligned along the effective rotation axis of the pulse sequence, and the effective frame rotates around this axis with the effective frequency. The interaction frames represent the single-spin frame that follows the pulse sequence and the cyclic frame, which is compensated for the rotation with the effective frequency.

To cope with complex pulse sequences, we transfer the description into the interaction frame of the single-spin Hamiltonian (represented by S and a tilde to signify that it represents an interaction-frame representation) through the unitary transformation

$$\widetilde{\hat{I}}_q^S = \widehat{U}^\dagger(t)\hat{I}_q\widehat{U}(t), \qquad \widehat{U}(t) = \hat{T}e^{-i\int_0^t \hat{H}_{ss}(t')dt'} \tag{A2}$$

for $q = x, y, z$.

For simplicity, we consider the Hamiltonian as piecewise time-independent by selecting appropriate time intervals, such that the Hamiltonian consists of piecewise rotations, which need not be of equal length. When using a sequence of rectangular pulses, the Hamiltonian is time-independent during each pulse, and the single-spin Hamiltonian will perform a rotation in the cyclic subspace spanned by $\hat{I}_x$, $\hat{I}_y$, and $\hat{I}_z$. If the pulse sequence uses shaped pulses, these need to be split into small time steps, where the shaped pulse can be considered time-independent. In the following, we consider a pulse sequence consisting of N pulses and a total length t_M. Using a vector representation of the Hamiltonian, we can express the rotation axis for pulse element p at time t_p by a vector in the ($\hat{I}_x$, $\hat{I}_y$, $\hat{I}_z$)-space,

$$\vec{u}_p = \frac{1}{L_p}\begin{pmatrix}\omega_{\mathrm{rf}}(t_p)\cos\theta(t_p)\\ \omega_{\mathrm{rf}}(t_p)\sin\theta(t_p)\\ \Omega\end{pmatrix}, \tag{A3}$$

where $L_p = (\omega_{\mathrm{rf}}^2(t_p) + \Omega^2)^{1/2}$ ensures that the vector is normalized. The rotation angle is given by $\chi_p = L_p\Delta t_p$, where Δt_p is the length of the pulse element. The propagator in Eq. (A2) can easily be established from the piecewise time-independent pulse elements,

$$\hat{U}(t_i) = e^{-iH_{ss}(t_{i-1})\Delta t_{i-1}}\ldots e^{-iH_{ss}(t_1)\Delta t_1}e^{-iH_{ss}(0)\Delta t_0}, \tag{A4}$$

and we can calculate the time-dependent evolution of the single-spin operators in the interaction-frame using Eq. (7). The propagator in Eq. (A1) may be represented by a vector in the ($\hat{I}_x$, $\hat{I}_y$, $\hat{I}_z$)-space describing the overall rotation of all pulse elements (*vide infra*).

In the vector representation, a unitary transformation, e.g., the coordinate transformation from the rotating frame to the interaction frame, may be described as a matrix-vector product

$$\begin{pmatrix}\vec{u}_x^S\\ \vec{u}_y^S\\ \vec{u}_z^S\end{pmatrix}(t) = R^{SR}(t)\begin{pmatrix}\vec{u}_x^R\\ \vec{u}_y^R\\ \vec{u}_z^R\end{pmatrix}, \tag{A5}$$

where $R^{SR}(t)$ is a 3×3 rotation matrix that combines the piecewise rotations of the pulse sequence and $\vec{u}_q^X$ are the unit vectors describing the orientation of the $q = x, y, z$ axes of the frame $X = R$ or S. The superscript SR refers to the rotation matrix that transforms from the rotating frame (R) to the single-spin interaction frame (S), i.e., SR may be seen as $S \leftarrow R$. It should be noted that the opposite transformation from the interaction frame to the rotating frame may be performed by the transposed matrix $R^{RS} = (R^{SR})^T$. We may use Eq. (A5) to establish the relation between the spin operators in the rotating frame, $\hat{I}_s$, to the single-spin interaction-frame operators $\widetilde{\hat{I}}_s^S$ introduced in Eq. (A2).

2. The effective axis of rotation of the pulse sequence

To determine the effective axis of rotation for the entire pulse sequence and thereby establish an expression for $R^{SR}(t)$, we could investigate the form of the total propagator, $\hat{U}(t_M)$. However, it is difficult to retrieve the axis of rotation from the propagator, but rotation quaternions are a perfect means to capture the combined effect of sequential rotations.[34] The rotation quaternion may readily be established from $\vec{u}_p$ and χ_p for pulse element p [see Eq. (A3)],

$$\mathbf{q}_p = \cos\frac{\chi_p}{2} + (u_{p,x}\mathbf{i} + u_{p,y}\mathbf{j} + u_{p,z}\mathbf{k})\sin\frac{\chi_p}{2} \tag{A6}$$

in which the first term is called $q_{p,r}$ and the three latter terms are called $q_{p,i}$, $q_{p,j}$, and $q_{p,k}$. Using the quaternion description, it is straightforward to calculate the total rotation performed by the N elements of the pulse sequence

$$\mathbf{q}_{\mathrm{eff}} = \mathbf{q}_N\cdots\mathbf{q}_2\mathbf{q}_1 \tag{A7}$$

with the product calculated by normal quaternion arithmetics. $\mathbf{q}_{\mathrm{eff}}$ represents the total *effective* rotation performed by the pulse sequence and thus contains the same information as $\hat{U}(t_M)$ for a single spin. From the quaternion, we can find the rotation axis and rotation angle as

$$\vec{u}_{\mathrm{eff}} = \left(q_{\mathrm{eff},i}^2 + q_{\mathrm{eff},j}^2 + q_{\mathrm{eff},k}^2\right)^{-1/2}\begin{pmatrix}q_{\mathrm{eff},i}\\ q_{\mathrm{eff},j}\\ q_{\mathrm{eff},k}\end{pmatrix}, \qquad \chi_{\mathrm{eff}} = 2\arccos q_{\mathrm{eff},r}. \tag{A8}$$

These equations only hold if the net rotation is unequal to zero. In the case where the total rotation is a multiple of 2π, corresponding to zero net rotation, we simply define the effective axis to be along the z axis in the laboratory frame, $\vec{u}_{\mathrm{eff}} = (0, 0, 1)$. For

convenience, we also define the effective frequency, $\omega_{\text{eff}} = \chi_{\text{eff}}/t_M$. It is straightforward to establish the Cartesian rotation matrix from a quaternion

$$R(\mathbf{q}) = \begin{pmatrix} 1-2\left(q_j^2+q_k^2\right) & 2(q_iq_j-q_kq_r) & 2(q_iq_k+q_jq_r) \\ 2(q_iq_j+q_kq_r) & 1-2\left(q_i^2+q_k^2\right) & 2(q_jq_k-q_iq_r) \\ 2(q_iq_k-q_jq_r) & 2(q_jq_k+q_iq_r) & 1-2\left(q_i^2+q_j^2\right) \end{pmatrix}. \quad \text{(A9)}$$

Using this relation, we can see from Eqs. (A2) and (A5) that the matrix relating interaction-frame operators with the rotating-frame operators, $R^{RS}(t)$, is given by

$$R^{RS}(t_i) = \left(R\left(\mathbf{q}_{i-1}\right)\right)^T \ldots \left(R(\mathbf{q}_2)\right)^T \left(R(\mathbf{q}_1)\right)^T. \quad \text{(A10)}$$

We have now introduced three different ways to calculate the propagation of the spin system using (i) propagators, (ii) quaternions, or (iii) Cartesian rotation matrices. These three methods are completely equivalent but have different advantages. Propagators involve the Hilbert-space matrices or product operators and generally allow the best analytical insight into well-behaved cases, quaternions are perfect for finding the effective rotation as outlined above, and we find that rotation matrices provide good insight into the time dependencies of the rotations and we will rely much on them in the remaining part of the Appendix.

3. Single-spin operators in the flipped frame

Knowing the effective axis of rotation of the pulse sequence, we now define a flipped coordinate system (F) that has its z axis aligned with $\vec{u}_{\text{eff}}$. To effectuate this, we define the rotation quaternion $\mathbf{q}^{FR}$ that relates the rotating frame to the flipped frame. This is achieved through the cross product between the z axes of the two frames (recall that $\vec{u}_z^R$ represents the z axis of the rotating frame),

$$\begin{pmatrix} q_i^{FR} \\ q_j^{FR} \\ q_k^{FR} \end{pmatrix} = \frac{\vec{u}_z^R \times \vec{u}_{\text{eff}}}{|\mathbf{q}^{FR}|}, \qquad q_r^{FR} = \frac{1+\vec{u}_z^R \cdot \vec{u}_{\text{eff}}}{|\mathbf{q}^{FR}|}. \quad \text{(A11)}$$

From this quaternion, we can obtain the rotation matrix R^{FR} from Eq. (A9). The new set of single-spin operators will be given by the transformation

$$\begin{pmatrix} \hat{I}_x^F \\ \hat{I}_y^F \\ \hat{I}_z^F \end{pmatrix} = R^{FR} \begin{pmatrix} \hat{I}_x \\ \hat{I}_y \\ \hat{I}_z \end{pmatrix}. \quad \text{(A12)}$$

Combining Eqs. (A5) and (A12), we can express the interaction-frame operators in terms of the effective-frame operators,

$$\begin{pmatrix} \widetilde{\hat{I}}_x^S \\ \widetilde{\hat{I}}_y^S \\ \widetilde{\hat{I}}_z^S \end{pmatrix}(t) = R^{SR}(t) R^{RF} \begin{pmatrix} \hat{I}_x^F \\ \hat{I}_y^F \\ \hat{I}_z^F \end{pmatrix}. \quad \text{(A13)}$$

It is convenient to express the system in the flipped frame, since the effective rotation of a pulse sequence occurs around z^F. This implies that the component of the interaction-frame operators along z^F is cyclic with the period t_M and that the x^F and y^F components mix due to the rotation with frequency ω_{eff}. We now introduce the effective coordinate system represented by $\hat{I}_x^E$, $\hat{I}_y^E$, and $\hat{I}_z^E$, where

$$\begin{pmatrix} \hat{I}_x^E \\ \hat{I}_y^E \\ \hat{I}_z^E \end{pmatrix}(t) = R^{EF}(t) \begin{pmatrix} \hat{I}_x^F \\ \hat{I}_y^F \\ \hat{I}_z^F \end{pmatrix}, \qquad R^{EF}(t) = \begin{pmatrix} \cos\omega_{\text{eff}}t & -\sin\omega_{\text{eff}}t & 0 \\ \sin\omega_{\text{eff}}t & \cos\omega_{\text{eff}}t & 0 \\ 0 & 0 & 1 \end{pmatrix}, \quad \text{(A14)}$$

providing the relation

$$\begin{pmatrix} \widetilde{\hat{I}}_x^S \\ \widetilde{\hat{I}}_y^S \\ \widetilde{\hat{I}}_z^S \end{pmatrix}(t) = R^{SR}(t) R^{RF} R^{FE}(t) \begin{pmatrix} \hat{I}_x^E \\ \hat{I}_y^E \\ \hat{I}_z^E \end{pmatrix}. \quad \text{(A15)}$$

4. Time-dependency of rotation matrices

Up to now, we have managed to write the time-dependencies of any given single-spin operator in the single-spin interaction frame (S) as described in a so-called effective coordinate system. This is convenient since the total rotation of a pulse sequence (and chemical shift) corresponds to a rotation around the z axis of this frame. By going into the flipped frame (F) and afterward rotating, all three interaction-frame operators $(\widetilde{\hat{I}}_q^S, q = x, y, z)$ are cyclic with period t_M when described in the effective frame. As seen from Eq. (A15), the total transformation from the interaction frame to the effective frame is carried out by the rotation matrix $R^{ES}(t) = R^{EF}(t)R^{FR}R^{RS}(t)$. Because of the cyclic properties, we may describe the entries of this rotation matrix as Fourier components in terms of the characteristic frequency $\omega_M (= 2\pi/t_M)$,

$$R_{q,q'}^{ES}(t) = \sum_{k=-\infty}^{\infty} a_{q,q'}^k e^{ik\omega_M t} \quad \text{(A16)}$$

for all combinations of q, $q' = x, y, z$ with a^k representing the kth Fourier component (not a to the power k). It is noted that $R_{q,q'}^{ES}(t)$ is a real number, so $a_{q,q'}^k = \left(a_{q,q'}^{-k}\right)^*$.

5. Decomposition of time-dependencies

It is convenient to express the system in the flipped frame, since the effective rotation of a pulse sequence occurs around z^F with the frequency ω_{eff}. In NMR, rotations around z are routinely handled by going into the rotating frame of reference from the laboratory frame. The result of such a transformation is the removal of the term of the Hamiltonian responsible for this rotation, as it cancels with the Coriolis term due to the interaction-frame transformation. Likewise, to remove the effective rotation of a pulse sequence, we can enter an interaction frame that follows the effective cyclic rotation of the pulse sequence, the frame called C in Fig. 5, by the transformation

$$\widetilde{\hat{I}}_q^C = \hat{U}^\dagger(t)\widetilde{\hat{I}}_q^S\hat{U}(t), \qquad \hat{U}(t) = e^{-i\omega_{\text{eff}}t\hat{I}_z^F}. \quad \text{(A17)}$$

In the Cartesian-matrix formalism, this transformation can be written as

$$\widetilde{\hat{I}}^C = R^{CS}(t)\widetilde{\hat{I}}^S, \quad \text{(A18)}$$

but to express the rotation around z^F in the S frame, it is most convenient to transform from the S frame into the F frame, do the rotation, and then rotate back again,

$$\begin{aligned} R^{CS}(t) &= R^{SR}(t)R^{RF}\begin{pmatrix} \cos\omega_{\text{eff}}t & -\sin\omega_{\text{eff}}t & 0 \\ \sin\omega_{\text{eff}}t & \cos\omega_{\text{eff}}t & 0 \\ 0 & 0 & 1 \end{pmatrix}R^{FR}R^{RS}(t) \\ &= R^{SR}(t)R^{RF}R^{FE}(t)R^{FR}R^{RS}(t). \end{aligned} \quad \text{(A19)}$$

Here, we used the fact that the z-rotation has already been defined as the matrix $R^{FE}(t)$ in Eq. (A14). Merging this equation with Eq. (A13), we obtain

$$\begin{aligned}\widetilde{\hat{I}}^{C}(t) &= R^{CS}(t)R^{SR}(t)R^{RF}\begin{pmatrix}\hat{I}_x^F\\ \hat{I}_y^F\\ \hat{I}_z^F\end{pmatrix}\\ &= R^{SR}(t)R^{RF}R^{FE}(t)R^{FR}R^{RS}(t)R^{SR}(t)R^{RF}\begin{pmatrix}\hat{I}_x^F\\ \hat{I}_y^F\\ \hat{I}_z^F\end{pmatrix}\\ &= R^{SR}(t)R^{RF}R^{FE}(t)\begin{pmatrix}\hat{I}_x^F\\ \hat{I}_y^F\\ \hat{I}_z^F\end{pmatrix} = R^{SE}(t)\begin{pmatrix}\hat{I}_x^F\\ \hat{I}_y^F\\ \hat{I}_z^F\end{pmatrix}.\end{aligned} \tag{A20}$$

The matrix $R^{SE}(t) = (R^{ES}(t))^T$ has already been derived as a set of Fourier components in Eq. (A16). Combined with this, the latter expression in Eq. (A20) states that if we calculate the operators in the flipped frame, then the transformation into the $\tilde{C}$ frame may simply be described by the Fourier series in Eq. (A16). The advantage of expressing the matrix as a set of Fourier components is that it provides an easy means to evaluate conditions leading to constructive or destructive interference (resonance or nonresonance) when inspecting the coupling between two nuclei.

6. The J coupling

Merging the single-spin operators for two nuclei allows the reconstruction of the interaction-frame Hamiltonian. Transformation of the total Hamiltonian in Eq. (1) into the interaction frame defined by the two single-spin Hamiltonians, $H_{1,SS}$ and $H_{2,SS}$, leads to

$$\begin{aligned}\widetilde{\hat{H}}(t) =\ & \hat{U}_2^{\dagger}(t)\hat{U}_1^{\dagger}(t)\hat{H}\hat{U}_1(t)\hat{U}_2(t)\\ & -i\big(\hat{U}_1(t)\hat{U}_2(t)\big)^{\dagger}\frac{d}{dt}\big(\hat{U}_1(t)\hat{U}_2(t)\big),\\ \hat{U}_i(t) =\ & e^{-i\omega_{i,\mathrm{eff}}t\hat{I}_{i,z}^F}\hat{T}e^{-i\int_0^t \hat{H}_{i,ss}(t')dt'},\end{aligned} \tag{A21}$$

for $i = 1, 2$ and with the propagators defined as explicitly written, but not to confuse with previous definitions of propagators. The spin part of the J coupling term of the Hamiltonian in Eq. (1), $\hat{I}_1 \cdot \hat{I}_2 = \hat{I}_{1,x} \otimes \hat{I}_{2,x} + \hat{I}_{1,y} \otimes \hat{I}_{2,y} + \hat{I}_{1,z} \otimes \hat{I}_{2,z}$, transformed by individual transformations of the operators for the two spins by the propagator in Eq. (A21) implies that $\hat{U}_i^{\dagger}\hat{I}_{i,q}\hat{U}_i = \widetilde{\hat{I}}_{i,q}^C$. The Coriolis term in Eq. (A21) causes a net rotation around the z axis in the flipped frame, so

$$\widetilde{\hat{H}}(t) = -\omega_{1,\mathrm{eff}}t\hat{I}_{1,z}^F - \omega_{2,\mathrm{eff}}t\hat{I}_{2,z}^F + \pi J2\sum_{q=x,y,z}\widetilde{\hat{I}}_{1,q}^C \otimes \widetilde{\hat{I}}_{2,q}^C. \tag{A22}$$

Using Eq. (A20), we may rewrite the J-coupling term to yield

$$\begin{aligned}\widetilde{\hat{H}}(t) = & -\omega_{1,\mathrm{eff}}t\hat{I}_{1,z}^F - \omega_{2,\mathrm{eff}}t\hat{I}_{2,z}^F + \pi J2\\ & \times \sum_{q,q',q''=x,y,z}\big(R_{1,q,q'}^{SE}(t)\hat{I}_{1,q'}^F\big) \otimes \big(R_{2,q,q''}^{SE}(t)\hat{I}_{2,q''}^F\big).\end{aligned} \tag{A23}$$

From Eq. (A16), we already know that the Fourier series of $R^{ES}(t)$, and we also know that $R^{SE}(t) = (R^{ES}(t))^T$, hence

$$R_{q,q'}^{SE}(t) = \sum_{k=-\infty}^{\infty} a_{q',q}^k e^{ik\omega_M t}. \tag{A24}$$

The interaction-frame Hamiltonian provides good insight into the system under investigation. First, if the effective frequency is large, we will get a truncation around this axis similar to the truncation of J couplings created by chemical shift offsets. Furthermore, if we focus on the time-dependence of the J-coupling term, we notice that the time dependence is a modulation, corresponding to $e^{-ik_1\omega_M t}e^{-ik_2\omega_M t}$, where k_1 and k_2 are the indices of the infinite series for nuclei 1 and 2, respectively. Here, we will limit our discussion to the first-order averaged term, which requires $k_1 = -k_2$, implying that the first-order averaged interaction-frame Hamiltonian becomes

$$\begin{aligned}\bar{\widetilde{\hat{H}}}^{(1)} = & -\omega_{1,\mathrm{eff}}\hat{I}_{1,z}^F - \omega_{2,\mathrm{eff}}\hat{I}_{2,z}^F + \pi J\\ & \times \sum_{q,q',q''=x,y,z}\left(\sum_{k=-\infty}^{\infty} a_{1,q',q}^k a_{2,q'',q}^{-k}\right)2\hat{I}_{1,q'}^F \otimes \hat{I}_{2,q''}^F,\end{aligned} \tag{A25}$$

which holds for a homonuclear J coupling, while the sum over s should be reduced to $q = z$ for a heteronuclear coupling. This Hamiltonian is identical with the Hamiltonian in Eq. (3) of the Theory section.

The averaging in Eq. (A25) corresponds to the first-order term of the Magnus expansion, and the convergence is obviously a concern. We find that for the small J couplings encountered in this work, the first-order term is always sufficient to ensure convergence. A similar result was found for the much larger dipole-dipole interaction under magic-angle spinning.[30] However, convergence and the possible necessity for including higher-order terms is a concern in some cases and will be the subject of a future—ongoing—study.

For a given pulse sequence, we may readily calculate the effective frequencies for all single-spin Hamiltonians and for J-coupled spin pairs calculate the Fourier components to evaluate any surviving terms. In combination with the truncation due to the effective rotations, the Fourier components will allow us to easily calculate the scaling factor for the J coupling for any spin pair.

REFERENCES

[1] A. Abragam, *Principles of Nuclear Magnetism* (Clarendon Press, Oxford, 1983).
[2] A. G. Redfield, Adv. Magn. Opt. Reson. **1**, 1–32 (1965).
[3] O. W. Sørensen, G. W. Eich, M. H. Levitt, G. Bodenhausen, and R. R. Ernst, Prog. Nucl. Magn. Reson. Spectrosc. **16**, 163–192 (1984).
[4] F. S. de Bouregas and J. S. Waugh, J. Magn. Reson. **96**, 280–289 (1992).
[5] H. Bildsøe, STARS User's Guide, Spectrum Analysis for Rotating Solids, Publication No. 87-195233-00, Rev. A0296, Varian Associates, Inc., Palo Alto, 1996.
[6] M. Bak, J. T. Rasmussen, and N. C. Nielsen, J. Magn. Reson. **147**, 296–330 (2000).
[7] V. Macho, L. Brombacher, and H. W. Spiess, Appl. Magn. Reson. **20**, 405–432 (2001).
[8] D. Massiot, F. Fayon, M. Capron, I. King, S. Le Calvé, B. Alonso, J.-O. Durand, B. Bujoli, Z. Gan, and G. Hoatson, Magn. Reson. Chem. **40**, 70–76 (2002).
[9] M. Veshtort and R. G. Griffin, J. Magn. Reson. **178**, 248–282 (2006).
[10] M. H. Levitt, http://www.spindynamica.soton.ac.uk/; accessed 13 June 2017.
[11] H. J. Hogben, M. Krzystyniak, G. T. P. Charnock, P. J. Hore, and I. Kuprov, J. Magn. Reson. **208**, 179–194 (2011).
[12] L. Braunschweiler and R. R. Ernst, J. Magn. Reson. **53**, 521–528 (1983).
[13] A. Bax and D. G. Davis, J. Magn. Reson. (1969) **65**, 355–360 (1985).
[14] J. Briand and R. R. Ernst, Chem. Phys. Lett. **185**, 276–285 (1991).

[15]J. Cavanagh and M. Rance, J. Magn. Reson. **96**, 670–678 (1992).
[16]N. S. Bai and R. Ramachandran, J. Magn. Reson. A. **105**, 298–303 (1993).
[17]S. J. Glaser and G. P. Drobny, Chem. Phys. Lett. **164**, 456–462 (1989).
[18]P. Coote, W. Bermel, G. Wagner, and H. Arthanari, J. Biomol. NMR **66**, 9–20 (2016).
[19]A. Kirschstein, C. Herbst, K. Riedel, M. Carella, J. Leppert, O. Ohlenschläger, M. Görlach, and R. Ramachandran, J. Biomol. NMR **40**, 227–237 (2008).
[20]A. Mohebbi and A. J. Shaka, J. Magn. Reson. **94**, 204–208 (1991).
[21]R. Konrat, I. Burghardt, and G. Bodenhausen, J. Am. Chem. Soc. **113**, 9135–9140 (1991).
[22]P. Coote, K. E. Leigh, T.-Y. Yu, N. Khaneja, G. Wagner, and H. Arthanari, J. Chem. Phys. **141**, 024201 (2014).
[23]S. J. Glaser, J. Magn. Reson. A. **104**, 283–301 (1993).
[24]J. Huth and G. Bodenhausen, J. Magn. Reson. A. **114**, 129–131 (1995).
[25]E. R. P. Zuiderweg, L. Zeng, B. Brutscher, and R. C. Morshauser, J. Biomol. NMR **8**, 147–160 (1996).
[26]J. Klages, H. Kessler, S. J. Glaser, and B. Luy, J. Magn. Reson. **189**, 217–227 (2007).
[27]I. C. Felli, R. Pierattelli, S. J. Glaser, and B. Luy, J. Biomol. NMR **43**, 187–196 (2009).
[28]S. J. Glaser and J. J. Quant, Adv. Magn. Opt. Reson. **19**, 59–252 (1996).
[29]D. Abramovich, S. Vega, J. Quant, and S. J. Glaser, J. Magn. Reson. A. **115**, 222–229 (1995).
[30]R. Shankar, M. Ernst, P. K. Madhu, T. Vosegaard, N. C. Nielsen, and A. B. Nielsen, J. Chem. Phys. **146**, 134105 (2017).
[31]T. Vosegaard, A. B. Nielsen, J. M. Vinther, and N. C. Nielsen, http://books.pastis.dk/advanced.html?id=ab; accessed 18 September 2018.
[32]A. Messiah, *Quantum Mechanics* (North-Holland Publishing Co., Amsterdam, 1965).
[33]Z. Tošner, R. Andersen, B. Stevensson, M. Edén, N. C. Nielsen, and T. Vosegaard, J. Magn. Reson. **246**, 79–93 (2014).
[34]B. Blümich and H. W. Spiess, J. Magn. Reson. (1969) **61**, 356–362 (1985).